ELSEVIER

Journal of Chromatography A, 768 (1997) 283–294

JOURNAL OF CHROMATOGRAPHY A

# Displacement electrophoresis of ampholytes in a continuous pH gradient moving in a capillary with a non-constant cross-section[1]

Miroslava Šťastná, Karel Šlais*

*Institute of Analytical Chemistry, Academy of Sciences of the Czech Republic, 611 42 Brno, Czech Republic*

Received 12 July 1996; revised 12 November 1996; accepted 23 December 1996

**Abstract**

Our previous contribution described the construction and function of miniaturized automated instrumentation for displacement electrophoresis using a separation compartment consisting of a tapered channel coupled to a constant cross-section detection fused-silica capillary. In this work, the above instrumentation is used to study the separation and focusing of the zones of ampholytes during their movement on the background of continuous pH gradient generated by carrier ampholytes. Dependencies of the resolution of chosen colored low-molecular-mass ampholytes on the working parameters – including the length of the detection fused-silica capillary, concentration of counterion in the leading electrolyte, electric current, amount of carrier ampholytes and the analyte acidobasic properties – are evaluated. A reasonable speed of separation and resolution can be achieved at a potential drop over the separation compartment down to 200 V.

*Keywords:* Displacement electrophoresis; pH gradients; Ampholytes; Nitrophenols; Piperazineethanols

## 1. Introduction

In addition to the standard electrophoretic methods known as isotachophoresis (ITP) [1,2] or isoelectric focusing (IEF) [3–5], focusing methods which use the electrophoretic mobilization of a continuous pH gradient generated by synthetic carrier ampholytes are used for the determination of amphoteric substances like proteins in capillary electrophoresis. These methods which represent the transition between the conventional methods are named as ITP with carrier ampholytes [6–10] or capillary IEF (cIEF) with electrophoretic mobilization [11–13] or isotachophoresis–isoelectric focusing [14]. In these techniques, the ampholytes are simultaneously separated and focused in a pH gradient during their movement through the capillary.

To analyze a given amount of sample, a capillary with sufficient volume is needed. Column coupling or volume coupling is one approach to the solution of this problem [15–17]. Although the separation capacity is higher in this case, deterioration of the zones due to transfer between different cross-sections occurs and a long detection capillary and thus a high voltage has to be applied again to reestablish the steady state.

The use of a shallow tapered channel with continuous decrease of cross-section towards the detection point meets both the suitable high separation

*Corresponding author

[1] Paper presented at the 10th International Symposium on Advances and Applications of Chromatography in Industry, Bratislava, June 30–July 4, 1996.


*PII* S0021-9673(97)00059-9

capacity of the system and the relatively lower voltage needed for the separation. The theoretical model of the focusing processes in the tapered capillary was described recently [18–21]. The advantages predicted for a continuously tapered channel in comparison to the constant cross-section capillary include lower voltage and pressure drop and higher limiting peak capacity [22].

The instrumentation for capillary displacement electrophoresis (cDE) based on the tapered channel in the separation compartment and the evaluation of its function were described previously [23]. According to the theoretical model, the zones leave the tapered capillary close to the steady state and a short constant cross-section capillary coupled to the tapered channel should be sufficient to achieve the steady state in the detector [24]. To verify this, experiments with 5-cm and 1-cm long detection fused-silica capillaries were compared in this study.

To our knowledge, the studies of the influence of the working parameters on the separation performance in focusing with continuous pH gradients include only fragmentary statements on the alteration of the working parameters related to the design of the electropherograph, mainly for the separation of proteins using electroosmotic [25,26] or electrophoretic mobilization [27].

Although successful focusing of horse heart myoglobin (p*I* 6.8) was shown in our previous work [23], proteins are not optimal for the evaluation of the separation model and optimizing studies. Therefore, low-molecular-mass colored p*I* markers, prepared and described previously [28,29], were used as model substances in this work. Under the experimental conditions used these substances gave narrow Gaussian zones, which enabled evaluation of the performance of this method in terms of resolution. The aim of this work was to study the influence of experimental parameters such as length of the detection fused-silica capillary, counterion concentration in the leading electrolyte, electric current and injected amount of carrier ampholytes on the resolution of focused peaks.

## 2. Experimental

The automated miniaturized instrumentation and its function were described previously [23]. The instrument included three basic units: (i) microprocessor controlled liquid handling device which allowed the injection of working solutions into the separation compartment [30], (ii) on-column photometric detector using the optic fiber technology [31] and (iii) separation compartment including the detection fused-silica capillary of constant cross-section coupled to the tapered channel manufactured from transparent organic glass. Schematically, the separation compartment is presented in Fig. 1. The inner diameter of the tapered channel (4) decreased from 0.8 to 0.4 mm with a total volume of 3 μl. Detection fused-silica capillaries (5) with an inner diameter of 0.25 mm and lengths to the detector of either 5 cm (2.5 μl) or 1 cm (0.5 μl) were used.

The electrodes in reservoirs of the leading electrolyte (LE) (6) and the terminating electrolyte (TE)

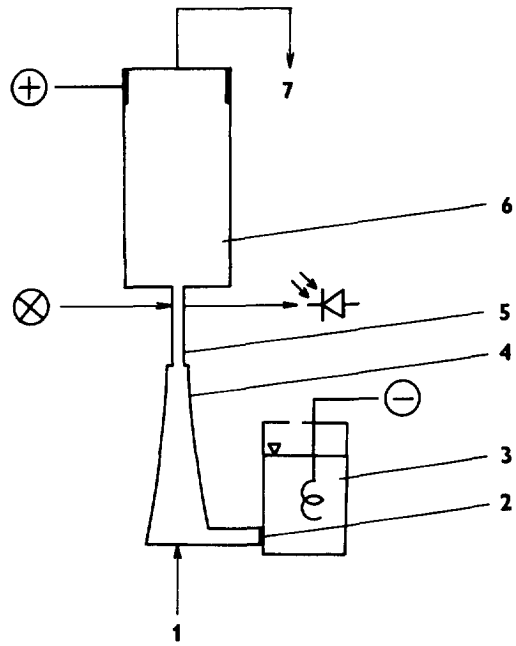


Fig. 1. Scheme of separation compartment of the instrument. (1) Inlet of the working electrolytes (leading electrolyte, sample, carrier ampholytes and transport liquid); (2) membrane with active area of 1 $mm^2$; (3) reservoir of the terminating electrolyte of volume 2 ml; (4) tapered channel of volume 3 μl (the inlet 0.8 mm I.D., the outlet 0.4 mm I.D.); (5) detection fused-silica capillary of volume to the detector either 2.5 μl (50 mm×0.25 mm I.D.) or 0.5 μl (10 mm×0.25 mm I.D.); (6) leading electrolyte reservoir of volume 120 μl; (7) waste.

(3) were connected either to the modified power supply with a voltage limitation up to 1 kV or to the Spellman power supply (CZE 1000 R, New York, USA). A two-line recorder (TZ 4620, Laboratory Instruments, Prague, Czech Republic) was used for the registration of the voltage and detector signals.

The instrument worked in the closed mode with constant current from 7 to 20 μA with a total voltage up to 900 V or 200 V and the substances moved as anions. As shown previously [23], the instrument worked in various modes of cDE, with the discontinuous (individual spacers) and continuous (carrier ampholytes) pH gradient, with the formation of both square-wave zones and Gaussian zones of analytes. In the present study, the mode with Gaussian peaks of p*I* markers on the background of a continuous pH gradient generated by carrier ampholytes was used.

### 2.1. Chemicals

All chemicals were of analytical grade. Succinic acid, cetyltrimethylammoniumbromide (CTAB), glycerine were obtained from Lachema (Brno, Czech Republic), hydroxypropylcellulose (HPC) from EGA Chemie (Steinheim/Albuch, Germany) and 2-amino-2-methyl-1-propanol (AMP) from Sigma (St. Louis, MO, USA). The solution of carrier ampholytes Ampholine pH 3.5–10.0 was from Pharmacia (Uppsala, Sweden).

The low-molecular-mass coloured ampholytes (p*I* markers) 2,6-bis[(4-methyl-1-piperazinyl)methyl]-4-nitrophenol [95380-45-3] (**3**), 4,4′-[(4-hydroxy-5-nitro - 1,3 - phenylene) - biethylene)] - bis(1 - piperazineethanol) [153954 - 01 - 9] (**5**), 4 - nitro - 2(1 - piperidin - ylmethyl) - phenol [77802 - 91 - 6] (**7**), 2,6 - bis(4-morpholinomethyl)-4-nitrophenol [153954-02-0] (**8**), 4-methyl-2[(4-methyl-1-piperazinyl)methyl]-6 - nitrophenol [153954 - 03 - 1] (**9**), 4 - [2 - hydroxy - 5methyl - 3 - nitrophenyl)methyl] - 1 - piperazineethanol [153954-04-2] (**10**), 2,4-bis(4-morpholinomethyl)-6-nitrophenol [127396 - 53 - 6] (**11**), 2 - (4 - morpholinylmethyl) - 4 - nitrophenol [69245 - 79 - 0] (**15**), 4 - [(3 - chloro - 4 - hydroxy - 5 - nitrophenyl)methyl] - 1 - piperazineethanol [153954-10-0] (**18**) and 2-chloro-4-(4-morpholinylmethyl)-6-nitrophenol [153954-11-1] (**19**) were prepared in the Institute of Analytical Chemistry (Academy of Sciences, Brno, Czech Republic). The bold numbers of p*I* markers were in agreement to those referred to in Refs. [28,29], the numbers in the square brackets and the names of p*I* markers were consistent with those given in Chemical Abstracts (CA registry numbers).

Table 1 shows the p*I* markers and their $pK_a$ values indicating the dissociation constants below and above the isoelectric point of the respective p*I* marker, isoelectric points, p*I*, relative molecular masses, $M_r$, maximum absorption wavelength at the pH corresponding to their isoelectric point, $(\lambda_{max})_{pI}$, and the slope of the effective charge, *z*, versus pH at the isoelectric point, $-(dz/dpH)_{pI}$.

Table 1
List of applied p*I* markers[a]

| Marker no.[b] | $pK'_a$ | $pK''_a$ | p*I* | $M_r$ | $\lambda_{max,\ pI}$ (nm) | $-(dz/dpH)_{pI}$ ($pH^{-1}$) |
|---|---|---|---|---|---|---|
| **2** | 9.35 | 10.90 | 10.1 | 406 | 412 | 0.60 |
| **3** | 8.02 | 9.27 | 8.6 | 509 | 420 | 0.74 |
| **5** | 7.62 | 9.24 | 8.4 | 569 | 417 | 0.60 |
| **7** | 5.49 | 10.48 | 8.0 | 273 | 392 | 0.02 |
| **8** | 6.92 | 8.87 | 7.9 | 435 | 403 | 0.45 |
| **9** | 6.74 | 9.10 | 7.9 | 338 | 425 | 0.27 |
| **10** | 6.36 | 9.04 | 7.7 | 368 | 423 | 0.19 |
| **11** | 6.53 | 8.43 | 7.5 | 410 | 416 | 0.43 |
| **15** | 5.16 | 8.07 | 6.6 | 275 | 400 | 0.15 |
| **18** | 4.53 | 7.81 | 6.2 | 389 | 415 | 0.10 |
| **19** | 3.76 | 6.91 | 5.3 | 309 | 409 | 0.12 |

[a] Values taken from Refs. [28,29]. [b] Numbers correspond to Refs. [26,28].

### 2.2. Leading electrolyte

The solution of succinic acid and AMP as counter-ion was used as LE (pH ~4.4). AMP was chosen due to its high $pK_a$ to generate broad pH gradient. Such a buffer behaves as a strong electrolyte in acidic LE. So, the leading anion should be the weak acid to enable to buffer in LE. Therefore, succinic acid was chosen due to suitable $pK_a'$ and low mobility. Thus, we obtained a relatively small difference in the conductivity between LE and TE. Since many experiments were done over a longer time period, the use of the fused-silica detection capillary with coated inner surface would not ensure the required stability. Further, the exchange of this capillary is not quite simple in the described instrument. For these reasons we used dynamic coating of the fused-silica detection capillary to modify the effective charge on its inner surface and to control the electroosmotic flow by means of CTAB and HPC added to the LE. This approach was shown to give an acceptable reproducibility as was described previously [23].

### 2.3. Terminating electrolyte

The reservoir of TE was filled with 0.01 mol $l^{-1}$ AMP solution (pH 10.5).

### 2.4. Transport liquid

Distilled water containing 10% (v/v) glycerine was used as the transport liquid, which brought the sample and carrier ampholytes to the proper position in the separation compartment relative to the position of the conduit to the reservoir of the terminating electrolyte.

### 2.5. Sample

The model mixture of p*I* markers **3**, **15** and **19** and mixtures of p*I* markers **3**, **5**, **7**, **8**, **9**, **10**, **11**, **15**, **18** and **19** were used as the model samples in this study.

### 2.6. Carrier ampholytes

A 1.4% solution of Ampholine (pH 3.5–10.0) was used in most of the experiments.

## 3. Results and discussion

### 3.1. Control of electroosmosis by dynamic modification of the capillary surface

To obtain narrow peaks of p*I* markers and to minimize the electroosmotic flow in the detection fused-silica capillary, the optimum value of the CTAB concentration in the leading electrolyte had to be determined. The dependence of the resolution between peaks of p*I* markers **19** and **15**, $R_{s1,2}$, and p*I* markers **15** and **3**, $R_{s2,3}$, on the concentration of CTAB in the leading electrolyte with the various AMP concentration is presented in Fig. 2. The resolution, $R_s$, was calculated using the relationship:

$$R_s = \frac{\Delta t}{2(\sigma_1 + \sigma_2)} \quad (1)$$

where $\Delta t$ is the difference in migration times of two adjacent peaks and $\sigma_1$ and $\sigma_2$ are their standard deviations. The optimum CTAB concentration 0.1 mmol $l^{-1}$ was used in most of the analyses.

### 3.2. Influence of the length of the detection fused-silica capillary

The theory of the tapered channel found that only short constant cross-section capillary coupled to the tapered channel should be sufficient to achieve the steady state of the zones in the detector (see Eq. 24 and Fig. 5 in Ref. [24]). In order to verify this expectation, the next experiments were carried out. The analysis in the arrangement with the 1-cm long detection fused-silica capillary shown in Fig. 3 was compared to the analysis in the arrangement with the 5-cm long detection fused-silica capillary presented in Fig. 4 for the same conditions. Using a constant electric current of 20 μA and otherwise the same conditions, the maximum voltage needed for the complete separation was up to 900 V for the device with the 5-cm long fused-silica capillary and up to about 310 V for the arrangement with the 1-cm long fused-silica capillary. In the former case, the tapered channel contributed 55% to the total volume of separation compartment and only 3% to the total resistance. The electric field was 18 V $mm^{-1}$ in the detection capillary. In the latter case, the tapered

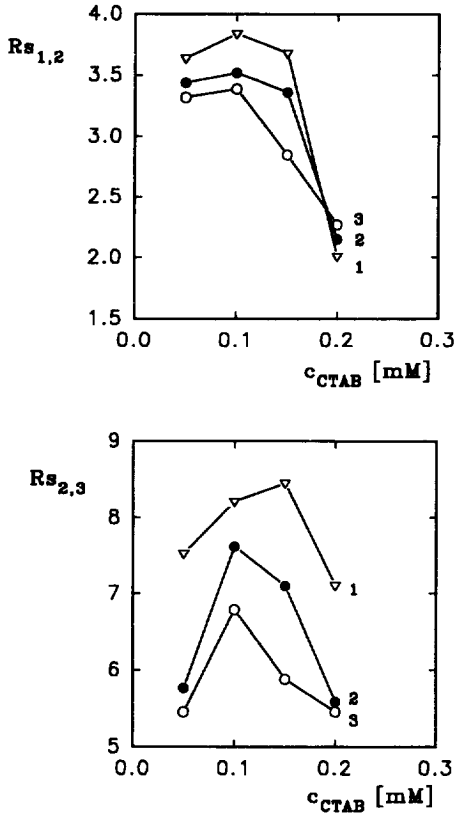


Fig. 2. Dependence of the resolution on the CTAB concentration in the leading electrolyte. $R_{s1,2}$, resolution between peaks of p*I* markers **19** and **15**; $R_{s2,3}$, resolution between peaks of p*I* markers **15** and **3**; $c_{CTAB}$, concentration of CTAB in the leading electrolyte; leading electrolyte: 10 mmol $l^{-1}$ succinic acid and 5 mmol $l^{-1}$ AMP (1) or 7 mmol $l^{-1}$ (2) or 8 mmol $l^{-1}$ (3), 0.06% (w/v) HPC; terminating electrolyte: 10 mmol $l^{-1}$ AMP; carrier ampholytes: 1.4% Ampholine (pH 3.5–10.0); injected volume of sample: 300 nl; injected volume of carrier ampholytes: 300 nl; $I=7$ μA; $\lambda=420$ nm; 1-cm long detection fused-silica capillary; modified power supply with voltage limitation up to 1 kV.

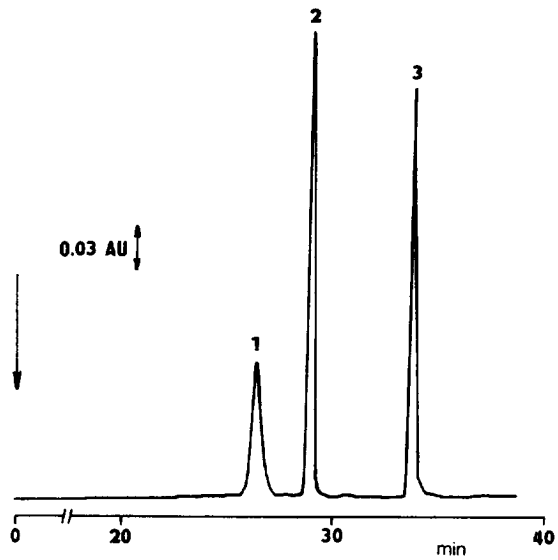


Fig. 3. Separation of p*I* markers in the arrangement with the 1-cm long detection fused-silica capillary. (1) p*I* marker **19** (0.32 mmol $l^{-1}$), (2) p*I* marker **15** (0.27 mmol $l^{-1}$), (3) p*I* marker **3** (0.20 mmol $l^{-1}$); leading electrolyte: 25 mmol $l^{-1}$ succinic acid and 17 mmol $l^{-1}$ AMP, 0.15 mmol $l^{-1}$ CTAB, 0.2% (w/v) HPC; terminating electrolyte: 10 mmol $l^{-1}$ AMP; carrier ampholytes: 1.4% Ampholine (pH 3.5–10.0); injected volume of sample: 300 nl; injected volume of carrier ampholytes: 1000 nl; $I=20$ μA; $\lambda=420$ nm; Spellman power supply.

channel contributed 86% to the total separation compartment volume and about 25% to the total voltage. The electric field was 23 V $mm^{-1}$ in detection capillary with considering of 25% of the total voltage drop over the tapered channel.

Further, the resolutions were calculated for both compared analyses. Resolutions $R_{s1,2}$ and $R_{s2,3}$ were 5.40 and 10.61 for the 5-cm long fused-silica capillary and 3.95 and 10.24 for the 1-cm long fused-silica capillary, respectively. Resolutions $R_{s1,2}$ and $R_{s2,3}$ became worse by about 25% and 3%. When we consider the 5-fold reduction of the detection capillary length, the decrease in the resolution of about 25% is no serious drawback in the former case and can be neglected in the latter case. In addition, it was calculated according to the equations describing the theoretical model [24] that steady state of the zones should be achieved in the 5-mm distance from the coupling point for the experimental conditions used. There is a step change in inner diameter between the narrower end of tapered channel [0.4 mm (4)] and the detection fused-silica [0.25 mm (5) (Fig. 1)] in our separation compartment. This transition in inner diameters causes departure from the steady state. Provided that by using a 5-cm long detection fused-silica capillary the zones are in steady state in detector (see calculation and comparison of theoretically calculated and observed peak standard deviations, [23]), the 1-cm long detection fused-silica capillary should reduce this departure of less than 0.001% according to Eq. (24) in Ref. [24]. Notwithstanding that many approximations had to be ap-

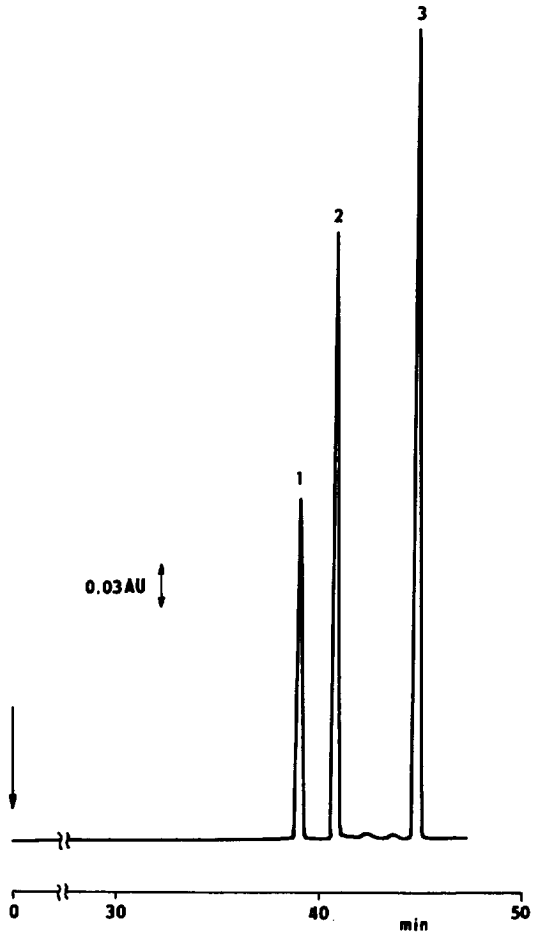


Fig. 4. Separation of p*I* markers in the arrangement with the 5-cm long detection fused-silica capillary. (1) p*I* marker **19** (0.22 mmol $l^{-1}$), (2) p*I* marker **15** (0.18 mmol $l^{-1}$), (3) p*I* marker **3** (0.13 mmol $l^{-1}$). Other experimental conditions are the same as in Fig. 3.

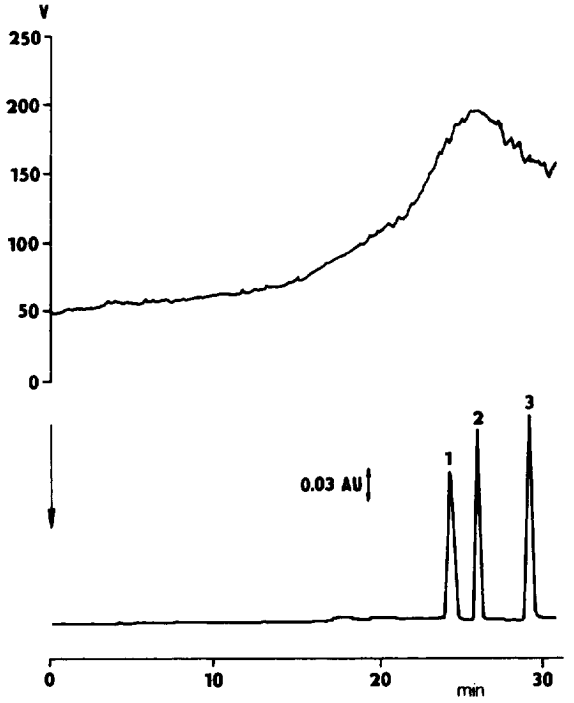


Fig. 5. Example of analysis of p*I* markers with the voltage course. (1) p*I* marker **19** (0.32 mmol $l^{-1}$), (2) p*I* marker **15** (0.12 mmol $l^{-1}$), (3) p*I* marker **3** (0.08 mmol $l^{-1}$); leading electrolyte: 10 mmol $l^{-1}$ succinic acid and 7 mmol $l^{-1}$ AMP, 0.1 mmol $l^{-1}$ CTAB, 0.06% (w/v) HPC; terminating electrolyte: 10 mmol $l^{-1}$ AMP; carrier ampholytes: 1.4% Ampholine (pH 3.5–10.0); injected volume of sample: 300 nl; injected volume of carrier ampholytes: 300 nl; $I=7$ μA; $\lambda=420$ nm; 1-cm long detection fused-silica capillary; modified power supply with voltage limitation up to 1 kV.

plied, a lower value of $R_{s1,2}$ could also be caused by other influences, e.g. by differences in electroosmosis on different surfaces of materials used.

### *3.3. Influence of counterion concentration in the leading electrolyte*

The following experiments illustrate the influence of counterion concentration in the leading electrolyte and, consequently, pH of LE on the resolution of focused peaks. The analysis of p*I* markers **19**, **15** and **3** is shown in Fig. 5 simultaneously with the voltage course. The maximum voltage needed was approximately 195 V for a constant current of 7 μA and the electric field in the 1-cm long detection fused-silica capillary was about 15 V $mm^{-1}$. The separation time was approximately 30 min.

Dependencies of resolutions $R_{s1,2}$ and $R_{s2,3}$ on the counterion AMP concentration are presented in Fig. 6 for two CTAB concentrations – 0.10 mol $l^{-1}$ and 0.15 mol $l^{-1}$ – in the leading electrolyte. Concentration of AMP counterion varied in the range 5–15 mmol $l^{-1}$, which corresponded to a pH of the leading electrolyte in the range 4.2–5.6 at a constant concentration of 10 mmol $l^{-1}$ of succinic acid in the LE. It can be see from Fig. 6 that the resolution increased with decreasing concentration of AMP. Moreover, it was found that the total voltage increased with

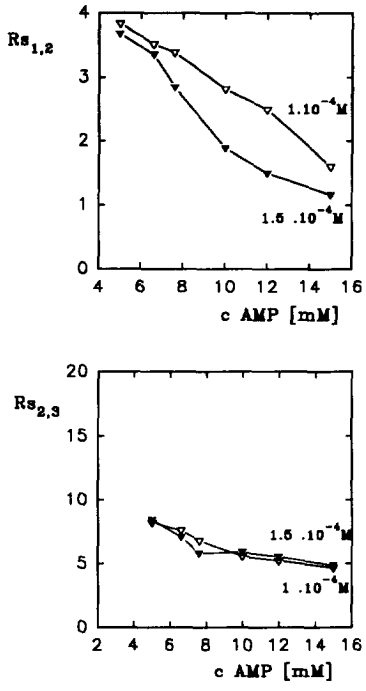


Fig. 6. Dependence of resolution on the counterion concentration in the leading electrolyte. $R_{s1,2}$, resolution between peaks of p*I* markers **19** and **15**; $R_{s2,3}$, resolution between peaks of p*I* markers **15** and **3**; $1 \cdot 10^{-4}$ *M* and $1.5 \cdot 10^{-4}$ *M*, depict CTAB concentrations in mol $l^{-1}$ in the leading electrolyte; $c_{AMP}$, concentration of AMP (counterion) in the leading electrolyte at the constant 10 mmol $l^{-1}$ succinic acid concentration. Other experimental conditions see Fig. 5.

decreasing AMP concentration as well. The separation time was slightly prolonged but could be considered as constant in comparison to the voltage growth. With respect to the isotachophoretic condition of constant migration velocity under the steady state, it means that the effective mobility of the zones decreased with decreasing AMP concentration in LE.

Since the effective mobility of a substance depends on its effective charge and in addition, the value of the dz/dpH slope and effective charge $z$ can change only a little, the main influence on the decrease of the effective mobility was the decreasing dissociation of substances, which caused the conductivity drop in the system and voltage increase. The $\sigma^2$ value decreased and the resolution increased with increasing voltage. For lower AMP concentration in LE, the voltage increased from the initial value given by conductivity of the leading electrolyte over the pH gradient to the maximum value (the increase was caused by lower dissociation and thus lower conductivity of the substances generating the pH gradient) and then decreased gradually to the value given by conductivity of the terminating electrolyte. The voltage increased from the leading electrolyte towards the terminating electrolyte without an observable maximum (the dissociation and the conductivity of the substances of the pH gradient was higher) for higher AMP concentrations in LE.

It should be noted that the relative positions of the p*I* marker peaks in the pH gradient were constant, which was checked by measurement of the migration time ratios of p*I* markers **15** and **19**, **3** and **19**. Thus, the resolution depended only on the change in the $\sigma$ value.

With a further decrease in the AMP concentration in LE, the peaks started to deform. Deformation was partly eliminated when the driving current was decreased from 7 μA to 3.5 μA. Dependencies of peak deformations on the decreasing AMP concentration in the range 4–2 mmol $l^{-1}$ in LE are illustrated in Fig. 7 at a constant electric current of 3.5 μA. These deformations were in the forms of split peaks. In contrast, deformations due to heat and/or electroosmosis resulted in tailing peaks. It could be

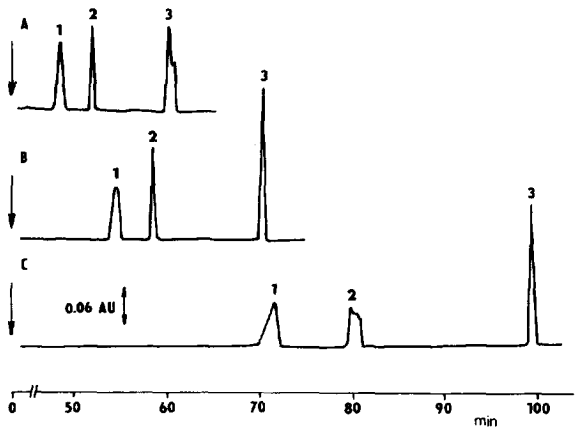


Fig. 7. Deformations of the peaks of p*I* markers for decreasing AMP concentration in the leading electrolyte. (1) p*I* marker **19**, (2) p*I* marker **15**, (3) p*I* marker **3**; leading electrolyte (10 mmol $l^{-1}$ succinic acid, 0.15 mmol $l^{-1}$ CTAB, 0.06% (w/v) HPC: (A) 4 mmol $l^{-1}$ AMP (pH 4.0), (B) 3 mmol $l^{-1}$ AMP (pH 3.9), (C) 2 mmol $l^{-1}$ AMP (pH 3.7); $I$=3.5 μA. Other experimental conditions see Fig. 5.

supposed that the peaks were split due to other reasons, e.g., by spacing of carrier ampholytes at non-regular intervals and/or by their smaller number in several parts of the pH gradient [1].

### 3.4. Influence of the electric current

In Fig. 8, the dependences of $R^2_{s1,2}$ and $R^2_{s2,3}$ on the increasing electric current for the ampholyte **19**, **15** and **3** are presented. The resolution increased with increasing electric current to a certain maximum value. Then the resolution and the separation efficiency decreased due to overheating by Joule heat [32]. Joule heat causes higher temperature and thereby faster migration velocities of the zones in the capillary axis, the zones become broader and resolution decreases. This course was in qualitative agreement with the observations in capillary zone electrophoresis (CZE), where the efficiency, expressed as the number of the theoretical plates $N$, was plotted against the intensity of electric field $E$ [33–36]. To show the similarity to CZE, the squared resolution was used. Because of constant conductivity in ZE, the dependence on $E$ means dependence on the electric current. The number of theoretical plates $N$ is inversely proportional to the variance $\sigma^2$. According to Eq. (1) in Section 3.1 squared resolution $R_s^2$ is inversely proportional to $\sigma^2$.

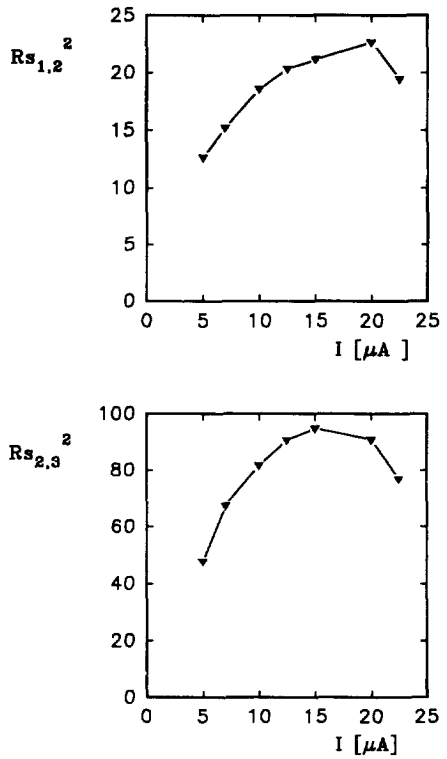


Fig. 8. Dependence of resolution on the electric current. $R^2_{s1,2}$, squared resolution between peaks of p*I* markers **19** and **15**; $R^2_{s2,3}$, squared resolution between peaks of p*I* markers **15** and **3**; *I*, electric current. Other experimental conditions see Fig. 5.

In quoted articles, either the 75-cm long fused-silica capillaries with 0.025 mm–0.1 mm I.D. were applied, thin capillaries ensured the good cooling and reduced heat effects [36] or the 1-m long glass capillaries were used with 0.75 mm I.D. at an applied voltage of 20 kV and an electric current of 0.1 mA [33]. Maximum possible heat power without overheating was about 2 W $m^{-1}$ in both cases.

In our work, the 1-cm long detection fused-silica capillary with 0.25 mm I.D. was used and a heat power of 0.7 W $m^{-1}$ was calculated for the maximum possible electric current of 15 μA corresponding to a voltage drop about of 500 V over the detection capillary. The value of the heat power corresponding to the maximum efficiency found here was in agreement with the above-mentioned articles, especially if we consider that a fused-silica capillary with 3-fold higher inner diameter related to [36] and glued into the organic glass with lower cooling efficiency was used. Improvement in our experimental arrangement with better cooling could be bring improvement in the resolution. The electric current of 7 μA applied in most of the experiments was suitable for routine measurements.

### 3.5. Influence of injected amount of carrier ampholytes

The dependences of injected amount of synthetic carrier ampholytes on the resolutions $R^2_{s1,2}$ and $R^2_{s2,3}$ were studied (Fig. 9). The theory of electrofocusing predicts that resolution increases with the square root of the pH gradient length. The pH gradient length is determined both by the concentration of the leading electrolyte which adjusts the concentration in the moving pH gradient and by the amount of carrier ampholytes [25]. According to the basic equation for the isoelectric focusing, the peak standard deviation, $\sigma$, increases with the square root of the gradient

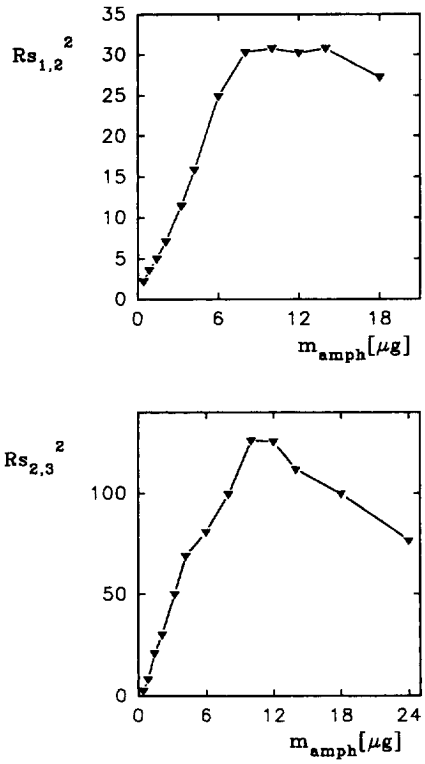


Fig. 9. Dependence of resolution on the amount of carrier ampholytes. $R^2_{s1,2}$, squared resolution between peaks of p*I* markers **19** and **15**; $R^2_{s2,3}$, squared resolution between peaks of p*I* markers **15** and **3**; $m_{amph}$ amount of carrier ampholytes in injected volume of 300 nl. Other experimental conditions see Fig. 5.

length as well as $R_s$ according to the equation for Gaussian peak resolution given in Section 3.1. It can be seen from the graphs in Fig. 9 that, as expected, the square of the resolution increased linearly up to some maximum value which corresponds to a certain amount of carrier ampholytes and then the separation efficiency dropped with a further increase in amount of background carriers. Since the volume of injected carriers was constant, the volume of the leading electrolyte and the time needed for migration from the injection point to the detection point remained the same in these experiments. The electric charge needed for separation and focusing of carrier ampholytes increases with the amount of carriers. For an amount of carrier ampholytes greater than the optimum value (about 10 μg in the injected 300-nl volume under the experimental condition used, see Fig. 9), the electric charge needed for separation was higher than that available during the zone migration between injection and detection point at the constant volume of the separation compartment and concentration of the leading electrolyte. Then, the substances could not be focused completely toward the steady state and the resolution decreased.

### *3.6. Influence of analyte pI and $(dz/dpH)_{pI}$ on the separation*

In IEF, the position of analyte in the pH gradient is given by its p*I*. In the focusing in the moving pH gradient, the analyte moves electrophoretically even under the steady state due to the non-zero effective charge of both carriers and analyte. So, the pH of the position of analyte is more or less different from its p*I*. The magnitude of this shift is indirectly proportional to the ampholyte $(dz/dpH)_{pI}$ value, the good ampholytes are shifted by few tenths of pH units [18]. Since low-molecular mass amphoteric dyes are used in this study, the influence of their acidobasic properties on the separation was examined.

Separation of a mixture of the p*I* markers **3**, **5**, **8**, **10**, **11**, **15**, **18** and **19** using 10 μg of carrier ampholytes injected in 300 nl of a 3.3% solution of carriers is presented in Fig. 10. The p*I* markers were ordered according to their increasing isoelectric points except p*I* markers **8** and **10** whose order was reversed. It follows from Table 1 that the difference between the isoelectric points of these p*I* markers was small (7.9 and 7.7) and the reversed order of separation was probably due to the different values of their slopes $|(dz/dpH)_{pI}|$ 0.45 and 0.19, respectively. With regard to the titration curves in Fig. 11, the ampholyte with smaller $|(dz/dpH)_{pI}|$ slope must have a larger distance from the isoelectric point than that with higher $|(dz/dpH)_{pI}|$ slope to have a certain effective charge and thus a certain effective mobility. So, that is why the ampholyte having a lower value of $|(dz/dpH)_{pI}|$ slope can overtake the ampholyte with a higher value of this slope although the value of its isoelectric point is lower. Consequently, p*I* marker **10** ocurred at a higher pH in the pH gradient compared to p*I* marker **8**. Although the relative molecular mass was higher for p*I* marker **8** ($M_r$ = 435, see Table 1), which should result in lower effective mobility in comparison to p*I* marker **10** ($M_r$ = 368), it must be concluded that the influence of

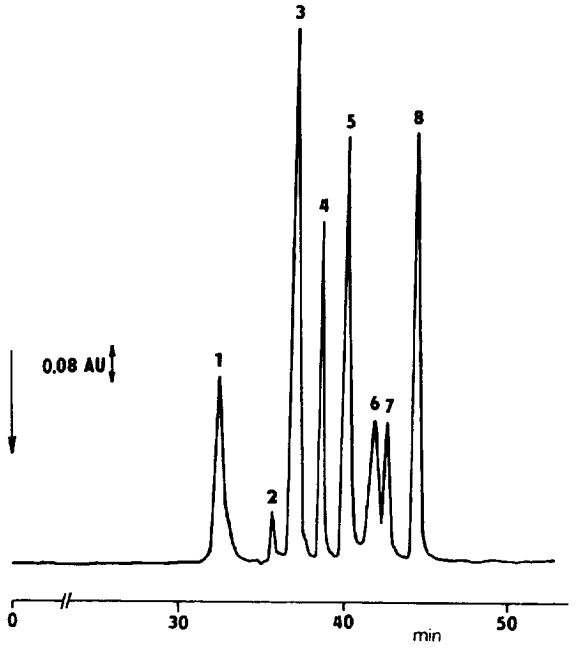


Fig. 10. cDE of mixture of p*I* markers. (1) p*I* marker **19** (0.20 mmol $l^{-1}$), (2) p*I* marker **18** (0.03 mmol $l^{-1}$), (3) p*I* marker **15** (0.23 mmol $l^{-1}$), (4) p*I* marker **11** (0.15 mmol $l^{-1}$), (5) p*I* marker **8** (0.14 mmol $l^{-1}$), (6) p*I* marker **10** (0.17 mmol $l^{-1}$), (7) p*I* marker **5** (0.11 mmol $l^{-1}$), (8) p*I* marker **3** (0.12 mmol $l^{-1}$); carrier ampholytes: 3.3% Ampholine (pH 3.5–10.0). Other experimental conditions the same as in Fig. 5.

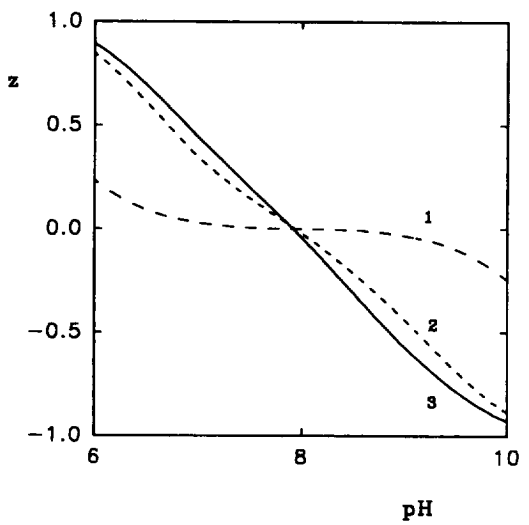


Fig. 11. Titration curves of p*I* markers **7**, **8** and **9**. (1) p*I* marker **7**, (2) p*I* marker **9**, (3) p*I* marker **8**; *z* effective charge of analyte.

relative molecular mass on the position of the compound in the pH gradient was much smaller than influence of the $(dz/dpH)_{pI}$ slope.

In order to illustrate this phenomenon more clearly, the following analysis of p*I* markers **3**, **7**, **8**, **9**, **15** and **19** was provided (Fig. 12). Experimental conditions were the same as in Fig. 10. Three p*I* markers **7**, **8** and **9** had the same or slightly different values of isoelectric points (8.0, 7.9 and 7.9, respectively) while their $|(dz/dpH)_{pI}|$ slopes differed markedly (0.02, 0.45 and 0.27, respectively). It can be seen from the records in Fig. 11 that these three p*I* markers were ordered according to their decreasing slope in direction of increasing pH in the pH gradient. Since the $|(dz/dpH)_{pI}|$ slope of the p*I* marker **7** is very low, this ampholyte was positioned beyond p*I* marker **3**, whose slope was 0.74 and isoelectric point at pH 8.6.

As the p*I* markers have similar relative molecular

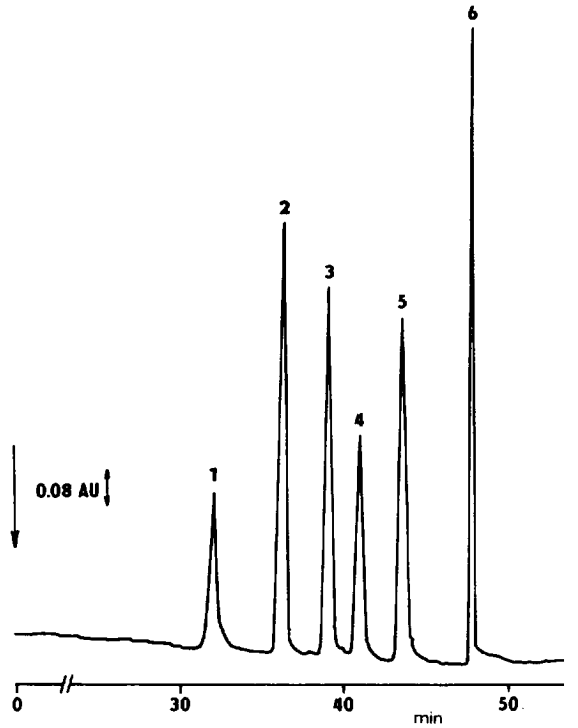


Fig. 12. cDE of mixture of pI markers. (1) p*I* marker **19** (0.13 mmol $l^{-1}$), (2) p*I* marker **15** (0.15 mmol $l^{-1}$), (3) p*I* marker **8** (0.10 mmol $l^{-1}$), (4) p*I* marker **9** (0.18 mmol $l^{-1}$), (5) p*I* marker **3** (0.08 mmol $l^{-1}$), (6) p*I* marker **7** (0.08 mmol $l^{-1}$). Other experimental conditions the same as in Fig. 10.

masses and the effective charge is differs enough from zero, separation according to $pK_a''$ can be assumed (see Figs. 10 and 12). Then, the behavior of p*I* markers in the moving pH gradient can be explained from the view of both ITP and focusing in the moving pH gradient.

## 4. Conclusions

The theoretical model of zone focusing in the pH gradient moving in the capillary with non-constant cross-section was derived recently [20–22,24]. To verify the theoretical model, the construction of the automated miniaturized instrumentation was provided and the function of the instrument was evaluated [23] by means of model low-molecular-mass ampholytes (p*I* markers) [28,29]. The dependences of resolution of three p*I* markers on the working parameters were evaluated. The parameters included the length of the detection fused-silica capillary coupled to the tapered channel in the separation compartment, the applied electric current, the concentration of counterion in LE and the amount of carrier ampholytes. The results obtained here were discussed with the background of the previous theory.

The electroosmotic flow was minimized by 0.1 mmol $l^{-1}$ concentration of CTAB in LE which was used throughout the study. It was shown that p*I* markers having the same or similar values of their isoelectric points can be separated according to their different slopes $(dz/dpH)_{pI}$. It was found and confirmed in this work and in our previous one [26] that the effective analyses of ampholytes with a separation efficiency comparable to the arrangement with the constant cross-section capillary can be realized by using the tapered channel with substantially smaller applied voltage during the analyses. To further improve the separation efficiency, the inner diameter of the detection fused-silica capillary coupled to the tapered channel and the detection cell volume should be decreased. These experiments are under preparation.

Presently, the trends towards miniaturization and decreasing of the detection limits are reflected, e.g., in analyses provided on glass chips in which a high voltage of tens of kilovolts can not be used. The low voltage causes low peak capacity on the chip. The use of a tapered channel which opens the possibility to design a separation compartment in which the peak capacity is not limited by the applicable voltage is promising.

## Acknowledgments

This work was partly supported by the Grant Agency of the Academy of Sciences of the Czech Republic, grant No. A 4031504.

## References

[1] F.M. Everaerts, J.L. Beckers and Th.P.E.M. Verheggen, Isotachophoresis, Elsevier, Amsterdam, 1976.
[2] P. Boček, M. Deml, P. Gebauer and V. Dolník, Analytical Isotachophoresis, VCH, Weinheim, 1988.
[3] J.C. Giddings and K. Dahlgren, Sep. Sci., 6 (1971) 345.
[4] H. Svensson, Acta Chim. Scand., 15 (1961) 325.
[5] P.G. Righetti, Isoelectric Focusing: Theory, Methodology and Applications, Elsevier Biomedical, Amsterdam, 1983.
[6] P. Delmotte, Sci. Tools, 24 (1977) 33.
[7] P. Delmotte, J. Chromatogr., 165 (1979) 87.
[8] S. Hjertén and M. Kiessling-Johansson, J. Chromatogr., 550 (1991) 811.
[9] F. Acevedo, J. Chromatogr., 470 (1989) 407.
[10] T. Manabe, H. Yamamoto and T. Okuyama, Electrophoresis, 10 (1989) 172.
[11] S. Hjertén and M. Zhu, J. Chromatogr., 346 (1985) 265.
[12] S. Hjertén, J. Liao and K. Yao, J. Chromatogr., 387 (1987) 127.
[13] S. Hjertén, K. Elenbring, F. Kilár, J.L. Liao, A.J.C. Chen, C.J. Siebert and M.D. Zhu, J. Chromatogr., 403 (1987) 47.
[14] T. Izumi, T. Nagahori and T. Okuyama, J. High Resolut. Chromatogr., 14 (1991) 351.
[15] F.M. Everaerts, Th.P.E.M. Verheggen and F.E.P. Mikkers, J. Chromatogr., 169 (1979) 21.
[16] Th.P.E.M. Verheggen and F.M. Everaerts, J. Chromatogr., 249 (1982) 221.
[17] V. Dolník, M. Deml and P. Boček, J. Chromatogr., 320 (1985) 89.
[18] K. Šlais, J. Microcol. Sep., 5 (1993) 469.
[19] K. Šlais, J. Chromatogr. A, 679 (1994) 335.
[20] K. Šlais, J. Chromatogr. A, 684 (1994) 149.
[21] K. Šlais, Electrophoresis, 16 (1995) 2060.
[22] K. Šlais, J. Microcol. Sep., 7 (1995) 127.
[23] M. Šťastná, V. Kahle and K. Šlais, J. Chromatogr. A, 730 (1996) 261.
[24] K. Šlais, J. Chromatogr. A, 730 (1996) 247.
[25] X.-W. Yao and F.E. Regnier, J. Chromatogr., 632 (1993) 185.

[26] J. Caslavska, S. Molteni, J. Chmelík, K. Šlais, F.Matulík and W. Thormann, J. Chromatogr. A, 680 (1994) 549.
[27] P. Delmotte, in Electrophoresis 1978, Elsevier North-Holland, 1978, p. 115.
[28] K. Šlais and Z. Friedl, J. Chromatogr. A, 661 (1994) 249.
[29] K. Šlais and Z. Friedl, J. Chromatogr. A, 695 (1995) 113.
[30] M. Krejčí and V. Kahle, J. Chromatogr., 392 (1987) 133.
[31] F. Foret, M. Deml, V. Kahle and P. Boček, Electrophoresis, 7 (1986) 430.
[32] S. Hjertén, Electrophoresis, 11 (1990) 665.
[33] J.W. Jorgenson and K.D. Lukacs, Anal. Chem., 53 (1981) 1298.
[34] J.W. Jorgenson and K.D. Lukacz, J. High Resolut. Chromatogr. Chromatogr. Commun., 4 (1981) 230.
[35] J.W. Jorgenson and K.D. Lukacz, J. Chromatogr., 218 (1981) 209.
[36] M.J. Sepaniak and R.O. Cole, Anal. Chem., 59 (1987) 472.